AIAA JOURNAL
Vol. 48, No. 2, February 2010

Jet Entrainment Theory for Vertical Takeoff and Landing Aircraft Suckdown

Paul Bevilaqua,* Richard Margason,† and Charles Gaharan‡
Lockheed Martin Aeronautics Company, Palmdale, California 93599

DOI: 10.2514/1.43258

The suckdown induced on a vertical takeoff and landing aircraft by the lift jets and the equal but opposite reduction of jet thrust have been studied to develop a physics-based model for predicting these forces. Static pressure distributions and jet velocity profiles have been computed and compared to surface pressure and jet survey measurements to understand the origin of the forces on the aircraft and jet. It is concluded that the suckdown force on the aircraft in the absence of flow separation is caused by the acceleration of the flow entrained by the jet; this acceleration reduces the static pressure on the bottom of the fuselage more than on the top of the fuselage. The equal but opposite reduction of jet thrust is due to the increased loss of jet kinetic energy to turbulence in the high-pressure region created at the nozzle exit by the turning of the entrained flow. It is shown that both forces can be computed correctly if the static pressure at the nozzle exit is allowed to adjust to the local static pressure imposed by the entrained flow.

Nomenclature

A_j	=	jet exit area, ft^2
C	=	doublet strength, ft^2/s
C_p	=	pressure coefficient, $(p\text{-}p_{\text{ref}})/q$
D	=	plate diameter, ft
d	=	jet diameter, ft
F	=	force, lbf
F_x	=	flow force at a distance x ft downstream from the nozzle exit, lbf
J	=	jet decay parameter
m	=	mass flow at a distance x ft downstream from the jet exit, slug/ft^3
m_e	=	entrained mass flow, slug/ft^3
m_j	=	jet exit mass flow, slug/ft^3
P	=	static pressure, psf
P_{ref}	=	reference pressure, psf
P_T	=	total pressure, psf
Q	=	sink strength, ft^2/s
q	=	dynamic pressure, psf
q_e	=	dynamic pressure at nozzle exit, psf
R	=	jet radius, ft
r	=	radial distance, ft
S	=	plate area or body area normal to the X axis, ft^2
s	=	distance between a pair of flow singularities, ft
T	=	thrust, lbf
T_T	=	total temperature, R
U	=	mean velocity in the x direction, fps
u'	=	turbulent component of the velocity in the x direction, fps
V	=	mean velocity in the radial direction, fps
X, Y, Z	=	Cartesian axes
x, r, θ	=	polar coordinates
x, y, z	=	Cartesian coordinates
Y^+	=	dimensionless boundary-layer wall parameter
ΔL	=	jet-induced lift loss, lbf
Δp	=	pressure difference, psf
ε	=	turbulence dissipation rate
κ	=	turbulence kinetic energy
μ	=	coefficient of viscosity,
ρ	=	density, slug/ft^3

Subscripts

e	=	nozzle exit
f	=	fuselage
j	=	jet
m	=	mixed flow
o	=	reference case after theoretical expansion to ambient pressure
tp	=	total pressure
x	=	streamwise
Δ	=	region of the flowfield where the pressure differs from the ambient pressure
∞	=	freestream at infinity
$*$	=	local thrust after theoretical expansion to ambient pressure

Introduction

ENTRAINMENT by the lift jets of a hovering vertical takeoff and landing (VTOL) aircraft induces a downwash over the aircraft's wings and fuselage. This downwash generates a drag that reduces the effective lift of the jets. The induced flow accelerates as it is entrained into the lift jets on the bottom of the aircraft, and this acceleration reduces the base pressure. If the induced flow separates from the wing and fuselage, the reduced static pressure in the separation zones also causes a significant base drag on the bottom of the aircraft. Skin friction due to the induced flow over the surface of the aircraft is negligible.

There have been several experimental investigations of jet-induced lift loss [1–8] that have provided a detailed body of experimental data. Gentry and Margason [5] measured the jet-induced suction forces on a flat plate. In the case of the infinite plate shown in Fig. 1, the jet induces a flow that causes a reduction in the surface static pressure over a plate located in the plane of the nozzle exit. The reduced pressures result in a force that causes a loss of lift. These data show that the induced suction pressure coefficient is increased as the nozzle pressure ratio is reduced. For the case of the

Presented as Paper 1397 at the 45th Aerospace Sciences Meeting, Reno, NV, 1–11 January 2007; received 16 January 2009; accepted for publication 8 September 2009.

*Manager, Advanced Development Programs, 1011 Lockheed Way MS 1122. Fellow AIAA.

†Senior Staff Aeronautical Engineer, 1011 Lockheed Way. Associate Fellow AIAA.

‡Manager, Propulsion Airframe Integration, 1011 Lockheed Way. Member AIAA.

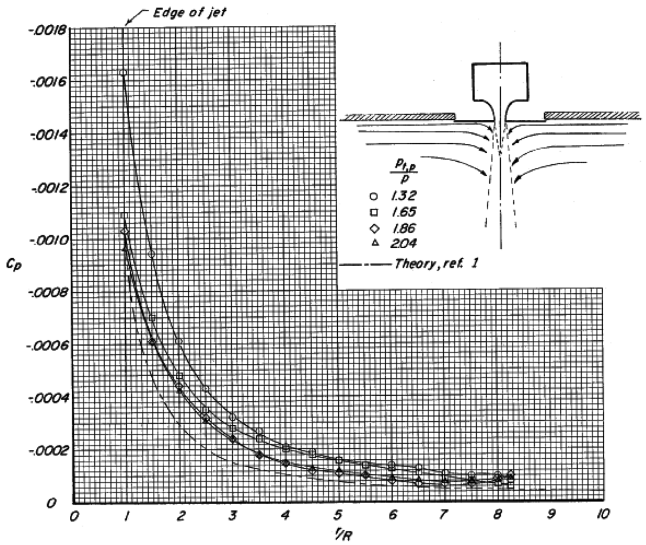

Fig. 1 Jet-induced suction pressures on an infinite flat plate from [5].

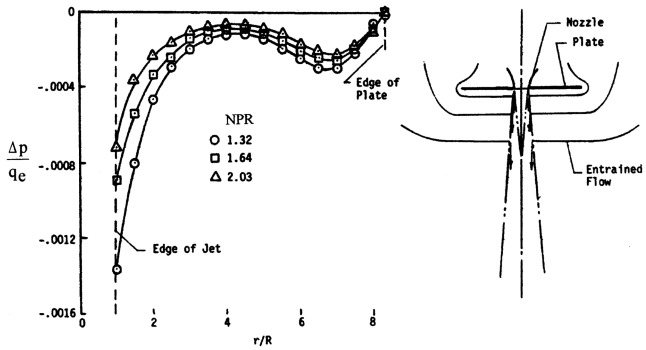

Fig. 2 Jet-induced suction pressures on a finite flat plate from [5].

finite flat plate shown in Fig. 2, the lift loss is aggravated by flow separation at the outer edge of the plate.

Measurements were made for several plate sizes and for several different jets. The results presented in Fig. 3 show that lift loss is proportional to the square root of the ratio of the plate area to the jet area. It also shows that the rate of decay depends on the shape of the nozzle and plenum chamber. The circular symbols represent a jet from a nozzle with a contraction ratio of 39, which results in low initial jet turbulence. The diamond symbols represent a jet driven from a small, rectangular plenum designed to fit inside a wind-tunnel model. Internal flow separation generated a high turbulence level, and the largest lift loss was measured. The triangular symbols represent the rectangular plenum with improved internal flow and a reduced lift loss. The square symbols represent flow from the round plenum with a balsa strut wedged across the jet as a blockage in the flow. The blockage increased the lift loss. An empirical correlation of lift loss as a function of a jet decay parameter was developed from these data. This relation is given as

$$\frac{\Delta L}{T} = -0.009\sqrt{\frac{S}{A_j}}J \tag{1}$$

in which the decay parameter is

$$J = \sqrt{-\left[\partial\left(\frac{q_x}{q_j}\right)\Big/\partial\left(\frac{x}{d}\right)\right]_{\max}\Big/\left(\frac{x}{d}\right)}$$

Data from Wyatt [2] are also shown for comparison. Subsequent measurements of the jet decay characteristics have confirmed that the lift loss increases with increasing entrainment.

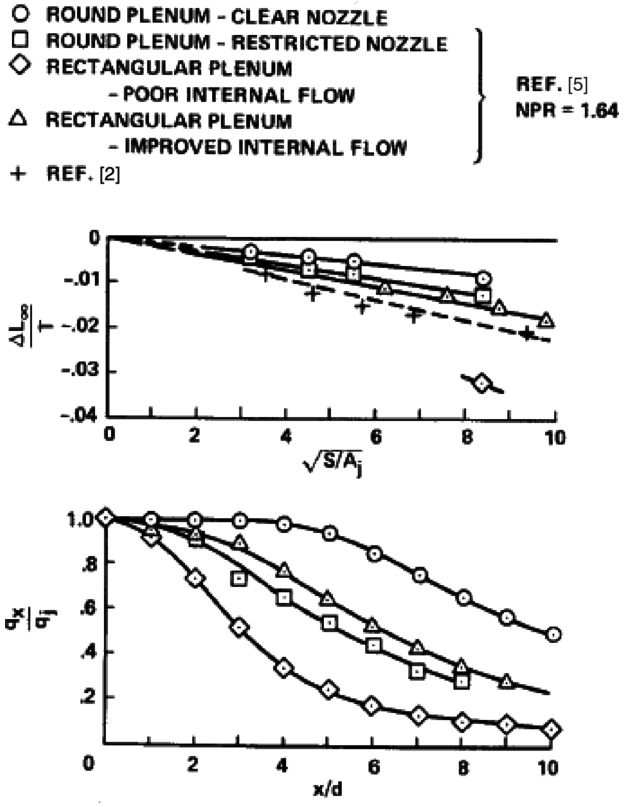

Fig. 3 Effect of jet characteristics on decay rate and on the lift-loss-induced out-of-ground effect [5].

For an airplane in ground effect, the magnitude of this suckdown force can be as much as half of the jet thrust, so that it is important to understand and control. But suckdown is very difficult to predict because it is highly dependent on the aircraft configuration, including the planform shape and the number of jets, as well as the aircraft's height above the ground. Because of the complexity of the flowfield, the best way to predict suckdown has been with scale-model tests. Empirical loss coefficients are used to scale the model data to the full-size aircraft. However, this approach represents just half of the jet/airframe interaction. Suckdown induces a force on the airframe, but the equal and opposite reaction is a reduction in the thrust of the jet. Empirical methods neglect this loss of jet thrust, even though it is important in predicting ground effects and the strength of the fountain jets that arise from the interaction of multiple lift jets on the ground.

The purpose of this paper is to describe the mechanism of this thrust loss and to investigate the use of computational fluid dynamics to model the equal and opposite forces of suckdown. The mechanism of thrust loss is described in the first part of this paper. The computational approach and turbulence model used are described in the next sections. The results of the computations are then compared to existing experimental data in the next-to-last section. In the last section, it is concluded that the loss of jet thrust can be correctly computed if the static pressure calculated at the nozzle exit is free to adjust to the local static pressure imposed by the entrained flow.

Potential Flow Model of Suckdown and Loss of Jet Thrust

The loss of jet thrust is due to the mixing between the lift jets and the atmosphere, due to the viscosity of the gases. However, the thrust is not lost to the friction between the jet and the atmosphere; rather, it is due to equal but opposite pressure forces induced on the aircraft and the lift jets. These forces can be understood by consideration of the potential flow outside the jet. Figure 4 shows the calculated streamlines of the flow entrained by an axisymmetric, turbulent lift jet. The jet originates from a point near the center of the figure and is directed downward, toward the bottom of the figure. The streamlines

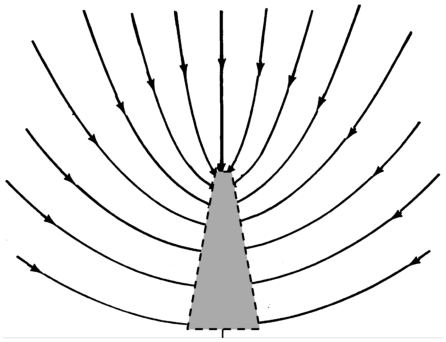

Fig. 4 Calculated streamlines of the flow being entrained by an isolated jet.

of the entrained flow were generated by distributing a line of sinks along the axis of the jet. The strength of the sinks varies as $x^{-1/2}$, corresponding to the streamwise variation in the rate of entrainment of a self-preserving axisymmetric jet. The boundary of the jet is indicated by the dotted lines. The narrowing of the stream tubes as the flow nears the jet centerline reflects the acceleration of the flow as it nears the jet. The spacing between the streamlines increases in the downstream direction, because the strength of the sinks is decreasing.

If the jet originates from a body, such as the fuselage cross section shown in Fig. 5, the acceleration of the flow as it nears the jet reduces the static pressure on the bottom of the fuselage more than it is reduced on the top of the fuselage. As a result, there is a net download on the fuselage. If the flow separates from the fuselage, the base pressure is further reduced and the suckdown forces increase.

Because the jet induces a pressure force on the body, the body must induce an equal but opposite force on the jet. Although this reaction force is due to the turbulent mixing between the lift jets and the surrounding atmosphere, it is conceptually similar to the ram drag experienced by a sink in an external stream. For example, consider the interaction between a source-sink pair representing the fuselage cross section, and a sink representing the entrainment by a section of the jet, as shown in Fig. 6. At the location of Q_f, the sink representing the fuselage, the sink representing the jet entrainment induces a velocity directed toward itself of magnitude

$$U_j = Q_j/2\pi s$$

where Q_j is the jet sink strength and s is the distance between the sinks. This results in a force of magnitude

$$F = Q_f U_j = Q_f(Q_j/2\pi s)$$

on the fuselage and directed toward the jet. This force represents the suckdown induced on the fuselage. It is shown by the down arrow in Fig. 6.

Similarly, the sink representing the fuselage induces a velocity at the jet sink directed toward itself of magnitude

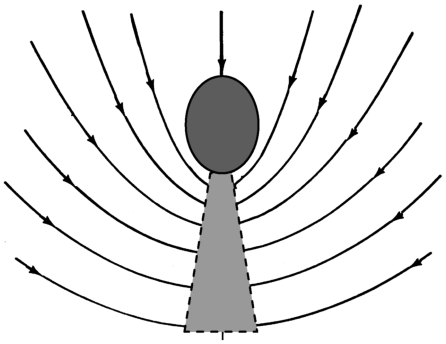

Fig. 5 Acceleration of the entrained flow induces a net download on the fuselage.

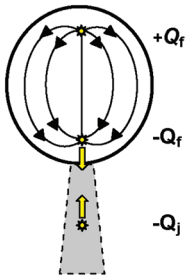

Fig. 6 Equal and opposite forces induced on sinks representing the fuselage and jet.

$$U_f = Q_f/2\pi s$$

where Q_f is the strength of the fuselage sink. This results in an equal but opposite force of magnitude

$$F = Q_j U_f = Q_j(Q_f/2\pi s)$$

on the jet and directed toward the fuselage. This is shown by the up arrow and represents the thrust loss induced on the jet.

The force on the source that is the other half of the fuselage source-sink pair in this simple example also experiences a force. Although this force reduces the suckdown and jet drag, it is smaller than the sink force because the source is farther from the jet than the sink. Therefore, the net forces are a suckdown and equal but opposite jet drag. Even in the limit as the distance between the source-sink pair is reduced until they become infinitely close together and form a doublet, the doublet induces a velocity at the jet sink directed toward itself of magnitude

$$U_f = C_f/2\pi s^2$$

where C_f is the strength of the doublet. The mutually induced forces create a suckdown on the body in this case, too. As long as the induced flow accelerates past the body, the pressure on the lower surface will be more negative than on the upper surface and the net force will be a suckdown.

Mechanism of the Jet Mixing Loss

Of course, this potential flow model is only an irrotational simulation of the actual mechanism of jet thrust loss due to entrainment and mixing. Jet mixing is essentially a collision between the jet and the surrounding air, so that it is governed by the same laws of momentum and energy conservation as any other collision. If the jet mixing occurs in a region of constant static pressure, as would be the case far from the aircraft, the thrust of the jet is conserved and some of its kinetic energy is dissipated due to the viscosity of the air. But, if the jet originates in a region where the static pressure, P_Δ, is different from the undisturbed pressure at infinity, P_∞, mixing changes the jet thrust by changing the dissipation of kinetic energy. The following simple analysis illustrates this phenomenon.

Within the region where the pressure, P_Δ, is different from atmospheric pressure, the velocities at the jet exit and in the coflowing entrained flow, before mixing, are assumed to be

$$U_{j\Delta} = [2(P_T - P_\Delta)/\rho]^{1/2} \quad \text{and} \quad U_\Delta = [U_\infty^2 + 2(P_\infty - P_\Delta)/\rho]^{1/2}$$

in which $P_\mathbf{T}$ is the stagnation pressure of the jet and U_∞ is the velocity of the freestream at infinity. Momentum is conserved during the mixing process itself so that

$$m_j U_{j\Delta} + m_e U_\Delta = (m_j + m_e) U_{m\Delta}$$

in which m_j is the initial mass flux of the jet, m_e is the quantity of mass entrained by the jet, and $U_{m\Delta}$ is the velocity of the mixed flow.

If the jet is then assumed to flow out of the mixing region where the static pressure is P_Δ into the region of undisturbed pressure, P_∞, without additional mixing, the change in the jet velocity is given by Bernoulli's equation, so that

$$U_m = [U_{m\Delta}^2 - 2(P_\infty - P_\Delta)/\rho]^{1/2}$$

The ratio of the final thrust of this mixed flow jet, $(m_j + m_e)\, U_m$ to $m_o U_o$, the thrust of the jet that would have been obtained if the nozzle had initially exhausted directly into the undisturbed far-field pressure P_∞, can be evaluated by substituting in turn for U_m, then $U_{m\Delta}$, and finally for $U_{j\Delta}$ and U_Δ. Performing these substitutions yields for this ratio

$$R = (m_j + m_e)U_m/m_o U_o$$
$$= [1 + 2M[(1 + P)^{1/2}(U^2 + P)^{1/2} - P] + M^2U^2]^{1/2} - MU$$

in which $M = m_e/m_o$ is the jet entrainment ratio, $U = U_\infty/U_o$ is the velocity ratio, and $P = 2(P_\infty - P_\Delta)/\rho U_o^2$ is the normalized pressure difference.

If there is no pressure change, then $P = 0$ and the solution reduces to that for free jet mixing, that is, $R = 1$ and the jet thrust is conserved. Similarly, if there is a pressure difference but no mixing between the jet and the surrounding air, then $M = 0$ so that $R = 1$ and the thrust is conserved in this case, also. However, if the pressure in the mixing region is greater than the ambient pressure ($P_\Delta > P_\infty$), then $R < 1$, and the thrust of the jet is reduced. For the case of a hovering VTOL airplane, $U_\infty = 0$, and the equation for the thrust ratio may be approximated by the simpler expression

$$R = 1 - 1/2MP^2$$

because M and P are usually small. This approximation shows that the jet thrust decreases with increasing entrainment and pressure difference.

Conversely, if the static pressure in the mixing region is below the ambient pressure, then mixing similarly increases the thrust of the jet. This is the mechanism of ejector thrust augmentation.

Computational Analysis

To demonstrate that this is the nature of the interaction between the jet and the airframe, we computed the development of turbulent lift jets from a sphere and from a flat plate, representing the fuselage and wing of an aircraft. The cases were all two-dimensional axisymmetric geometries for a jet out-of-ground effect and in a quiescent environment. The calculations were performed with the Metacomp Technology, Inc. CFD + + code [9]. This code was selected because it uses a preconditioned solution technique that enables stable computation of flowfields that have both high- and low-speed flows.

Rather than calculating the mixing and expansion of the flow in sequential steps as in the previous section, the computational scheme treats both mechanisms simultaneously, at each point of the grid. The calculated suckdown and thrust losses were compared with each other and with existing experimental data to obtain further insight into the nature of the jet/airframe interaction, especially the loss of jet thrust. The effects of the initial velocity profile, turbulence intensity, and grid size on the computed flowfield were investigated first.

Effect of Initial Velocity Profile

Impulsively started flows often create problems in computational fluid dynamic simulations. A fluid element positioned next to a solid surface with some relative velocity represents an unphysical initial condition. Compression (or rarefaction) waves tend to be generated near these surfaces in the first few steps of the simulation, which can lower stability if the relative velocity is sufficiently large and these waves become sufficiently steep. Without proper initialization, severe transients can occur in the numerical simulation, which is likely to delay convergence. For this reason, the jet exit and core region were initialized consistent with the jet exit flow boundary conditions. The region surrounding the jet was initialized consistent with a low-velocity flow. The simultaneous solution of these two regions was obtained using the preconditioned solution technique.

The jet velocity at the nozzle exit was specified as Mach 0.66. A uniform pressure and temperature are commonly specified as the initial conditions at a nozzle exit. Such a plug flow profile is representative of many laboratory investigations, such as that in [10], in which the experimental jet is generated from a plenum chamber with a well-designed nozzle contraction. However, the initial jet velocity profile generated by an aircraft engine is quite different from the low-turbulence, uniform jets generated under laboratory conditions. The engine efflux usually has a nonuniform velocity profile with swirl and, occasionally, regions of separated flow. To better represent actual jets from aircraft, the initial jet profile for these calculations was based on Musker's 1979 formulation [11]. This represents a developed nozzle flow with boundary-layer profiles for all mean flow and turbulence quantities. A boundary-layer thickness equal to 5% of the nozzle diameter was prescribed for the jet initial conditions.

Effect of Initial Turbulence Intensity

A two-equation cubic κ–ε turbulence model [12] was used to compute jet development, because it provides many of the advantages of a full Reynolds-stress transport model, without the associated computational cost to obtain a solution. The model used in this study includes nonlinear terms that account for normal-stress anisotropy, as well as swirl and streamline curvature effects. Including the effect of vortex stretching was found to provide a better fit to experimental jet flows for the conditions of the present investigation. Solutions were found to be insensitive to the initial length scale so this was set equal to the jet radius. The initial turbulence intensity in the jet was parametrically varied from 2 to 20% (Fig. 7). It was found that a turbulence intensity of 20% best represents the jet decay rate found experimentally in [5] and shown in Fig. 3. This intensity is typical of the turbulence intensity in fully developed jets and mixing layers [13]. A turbulence intensity of 2% was used in the outer flow region.

Effect of Grid Size

The computational geometry was an axisymmetric jet in a cylindrical volume. The length of the flowfield in the direction of jet flow was 40 diameters and the radius of the cylinder was 20 jet diameters. The axisymmetric geometry was selected to a obtain solution in such a large computational volume in a reasonable time. The sides of the wedge-shaped computational domain are planes of symmetry. On the outer boundaries outside of the jet, only the static pressure and temperature were specified, whereas the velocities were computed. The upper boundary allows entrainment into the flow domain and the downstream boundary allows the jet and entrained flow to exhaust from the flow domain. A circular plane on the upstream boundary was used to represent the case of a jet exiting from a wing hovering out-of-ground effect, as shown in Fig. 7. Because the plate was so large relative to the nozzle diameter, edge effects were not modeled. The flat plate was prescribed to be a viscous, adiabatic wall. A two-part structured grid was used to efficiently represent both the region of high-speed jet flow and the region of low-velocity entrained flow that surrounds the jet and extends to the far-field boundaries, as shown in Fig. 8.

As seen in Fig. 9, a sphere for which the diameter was twice the jet diameter was used as a representative body of finite size. It was also specified to have a viscous, adiabatic wall. For these calculations, the same grid topology used downstream of the nozzle exit was wrapped around the sphere and extended upstream of the nozzle exit a distance

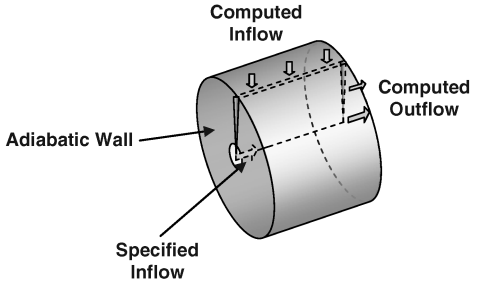

Fig. 7 Solution for the jet from a flat plate was obtained in a segment of the axisymmetric flowfield.

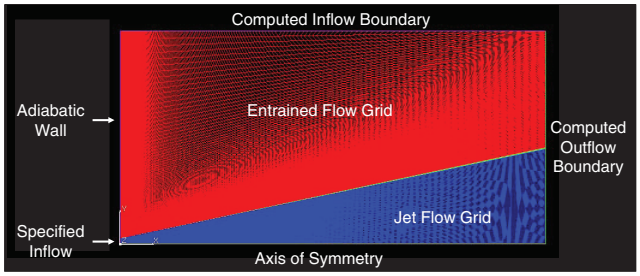

Fig. 8 Topology of the two part structured grid and the applied boundary conditions.

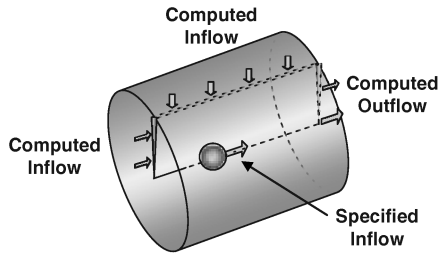

Fig. 9 Solution for the sphere was computed in a segment of the axisymmetric flowfield.

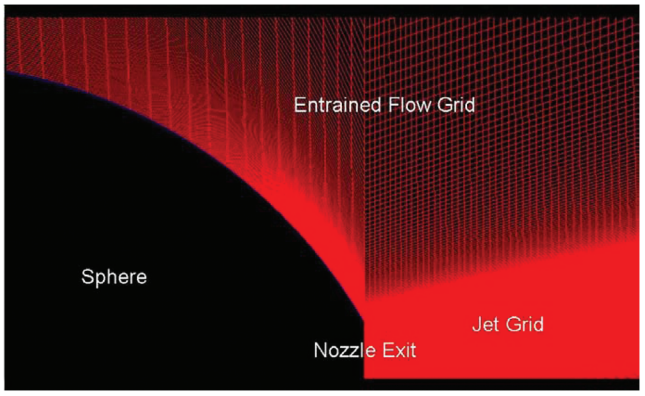

Fig. 10 Grid in the external flow was wrapped around the sphere and extended upstream.

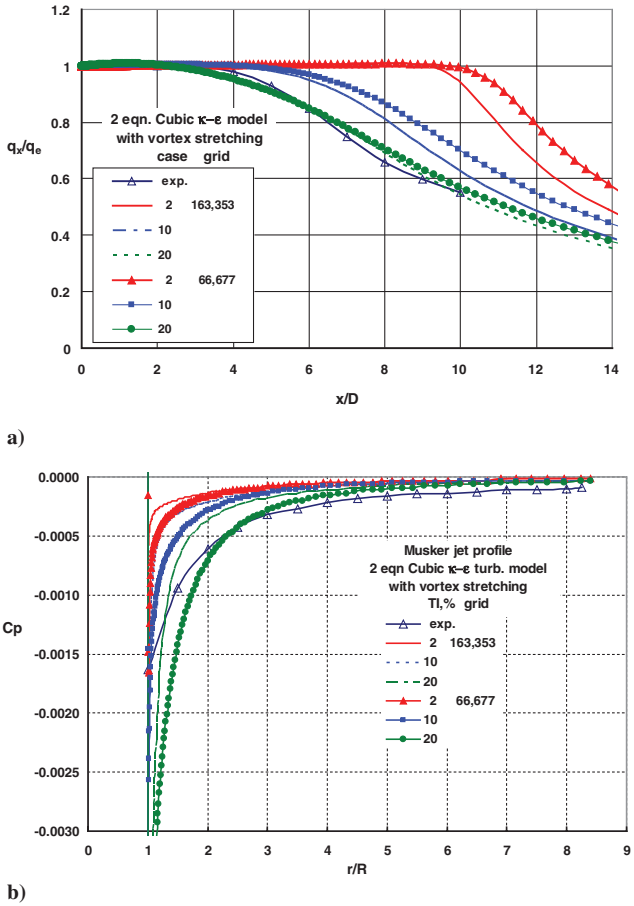

Fig. 11 Effects of grid size and turbulence intensity: a) jet decay, and b) wall surface pressures.

of 20 jet diameters, as shown in Fig. 10. The resultant grid included 203,154 cells. Four different grids were used to evaluate the effect of grid size, as shown in Table 1.

The effect of grid size is presented in Fig. 11 for the jet with turbulent intensities of 2, 10, and 20%. Although the residual for all of these cases converged in less than 500 iterations, some of the flows required additional iterations to converge. The convergence criterion was 10^{-4} for the maximum residual of the normalized transported quantities. Typical cases were run for 2000 iterations; in a few cases, especially for jet turbulent intensities of 20%, additional iterations were needed. In these cases, 4000–6000 iterations were computed to ensure that the solution was no longer changing.

The length of the potential core decreased as the jet turbulence intensity was increased. A turbulence intensity of 20%, representative of the turbulence intensity in fully developed jets and mixing layers, provided the best agreement with experimental data from [5]. It is also shown in Fig. 11a that the grid size had less effect on the computed rate of jet decay for large values of the turbulence intensity. With a turbulence intensity of 20%, increasing the grid size beyond 66,677 cells did not change the computed results. This is probably because, when the dissipation due to turbulence becomes large, it overshadows the numerical dissipation, which is a function of the grid size.

As shown in Fig. 11b, the experimental pressure coefficient data by Gentry and Margason [5] are more negative than the computed results in which $r/R < 2.5$. This is possibly because the experimental results were performed in a small room and the computational results are for a large computational domain. The investigation by Wyatt [2] measured a larger lift loss out-of-ground effect than measured in [5]. Later studies [3,4,6–8] showed some differences in the measured lift loss. For example, Shumpert and Tibbetts [3] found an effect due to nozzle pressure ratio and added a term to the correlation to account for the nozzle pressure ratio. These and other measurements were compared in Fig. 12 in [6], in which the out-of-ground effect lift loss was found to be affected by the size of the test chamber. The test cell volumes for both [5,6] (with door closed) were about 9000 ft^3 (the typical test cell dimension was about 100 jet diameters) and the high bay area of the NASA Ames Research Center 40 × 80 ft wind tunnel was over 6×10^6 ft^3 (the typical test cell dimension was

Table 1 Four grid sizes evaluated

Grid	Y^+ boundary-layer parameter	Number of jet cells radial x length	Number of outer region cells	Total number of cells
ax1	25	75 × 300	44,177	66,677
bx1	20	349 × 300	58,653	163,353
cx3	0.7	425 × 400	98,527	268,527
cx1b	0.5	699 × 600	237,703	657,103

about 1000 jet diameters). The data from the test cell in [5] and from the closed test cell in [6] showed similar lift losses. When the door at the end of the test cell in [6] was opened, the lift loss was significantly reduced.

There is a large body of steady and unsteady hot-wire data measured in low-turbulence axisymmetric jets by Z. D. Husain and A.K.M.F. Hussain. They note that there are discrepancies in the average flow measurements in the large body of published flow data. One example of their results is presented in [10], in which the influence of the initial and boundary conditions are evaluated by making hot-wire measurements in a 12.7 cm air jet mounted in a test cell that was 30 by 15 by 3.5 m. This is a test cell in which the characteristic size is less than 100 jet diameters. This is small in comparison with the results of Kuhn et al. [6], in which the largest test cell was greater than 1000 jet diameters. They investigated the effect of the presence of a flat plate in the jet exit plane and found that the presence of the flat plate reduced the quantity of entrained flow. However, the mean velocity and turbulence intensity profiles and the streamwise spectra showed no dependence on the geometry of the plate in the jet exit plane. Babu and Mahesh [14] computed the effect of a plate in the jet exit plane on the jet-induced entrainment and also found that the presence of the flat plate reduced the magnitude of the entrained flow.

A later test at the NASA Ames Research Center 40×80 wind-tunnel high bay by Kuhn et al. [6] had the lowest lift loss. The lift loss measured by Wyatt [2] was more than twice as large as in any of the other data. However, Wyatt's test setup included large ducts that obstructed the airflow and aggravated blockage effects. To summarize, Kuhn et al. showed that the magnitude of the out-of-ground effect lift loss was affected by the plate size, the jet pressure ratio, the jet turbulence level, and the size of the test cell.

The data in Fig. 12 suggests that the empirical equation should be modified to account for the effect of room size on the ratio of the slope of the lift loss (the vertical axis) between the test cell of [5] and the 40×80 high bay. At pressure ratios below 2, the slope is reduced by half for data in the largest test cell. If a corresponding slope change is made in the empirical equation, the constant changes from -0.0090 to -0.0045. This new form of the equation provides an empirical estimate of the lift loss that would be measured in a very large test cell, which should better represent the forces on an aircraft in free air. This new constant will be used later in this paper to assess the agreement between the calculations and the more representative lift from the corrected empirical correlation. Based on the data of Kuhn et al. [6], the lower suction pressures calculated in the present investigation may be closer to what would be measured in a large test cell than data currently available from small test cells.

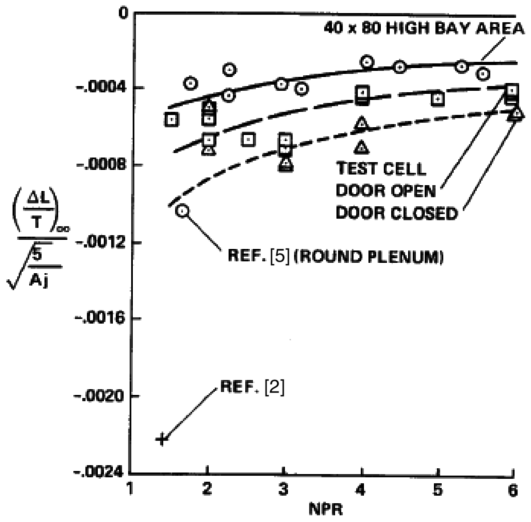

Fig. 12 Effect of the size of the test facility on the lift-loss-induced out-of-ground effect [6].

Results and Discussion

Jet from a Flat Plate

Figure 13 shows the computed results for the case of a jet exiting from a nozzle for which the exit is flush with the surface of a flat plate. The static pressure at infinity was specified to be 2116 psf and the total pressure of the jet was specified to be 2857 psf, which corresponds to a subsonic nozzle pressure ratio of 1.35. In the case shown, the static pressure at the nozzle exit was fixed at 2116 psf. However, the turning of the entrained flow as it enters the jet creates a high-pressure region downstream of the nozzle exit. The radial force balance in a stream tube of the entrained flow is

$$\Delta P = \rho w^2 s / R$$

where ΔP is the magnitude of the pressure rise, ρ is the density of the entrained flow, w is the local velocity of the entrained flow as it turns from essentially parallel to the plate to essentially parallel to the jet axis, s is the area of the stream tube, and R is the local radius of curvature of the stream tube.

Consequently, in Fig. 13a, the static pressure within the jet can be seen to rise from the fixed exit pressure of 2116 psf to a maximum value of about 2122 psf at a distance of about 1 diameter downstream from the jet exit. At greater distances downstream of the nozzle, the pressure slowly recovers to the ambient pressure. It is the mixing that occurs in the self-induced high-pressure region created by the turning of the entrained flow that reduces the thrust of the jet. Figure 13a was included here to show that the static pressure within the jet is made to rise by the turning of the entrained flow. For the results presented in this paper, the nozzle exit pressure was not constrained at 2116 psf, but was allowed to adjust to the pressure rise imposed by the turning of the entrained flow, as seen in Fig. 14a.

In Fig. 13b, the streamwise velocity U shows that the jet has a potential core about 5 diameters long. The jet then spreads at a half-angle of about 5.3 deg. This is consistent with the experimental data

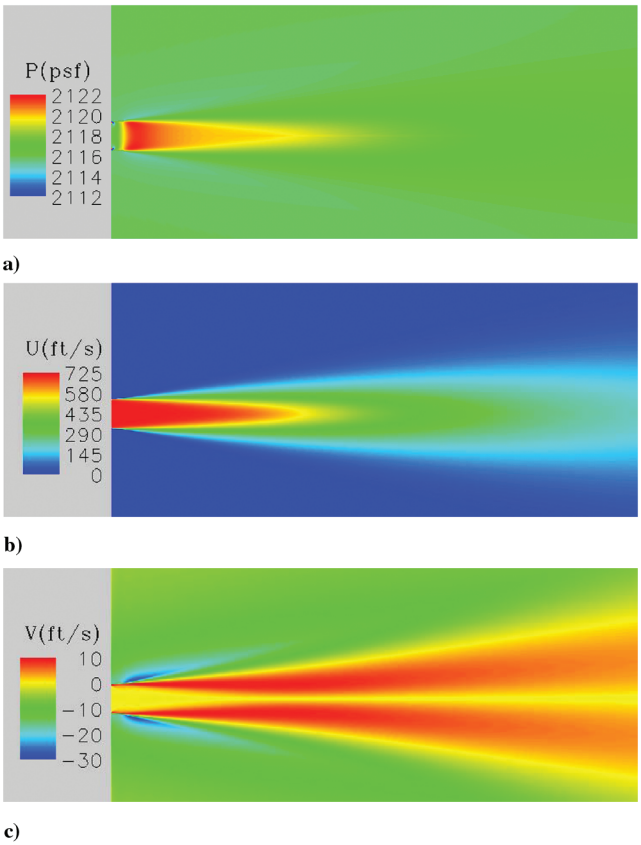

Fig. 13 Jet exiting a flat plate: a) static pressure with exit pressure constrained at 2116 psf, b) axial velocity, and c) radial velocity.

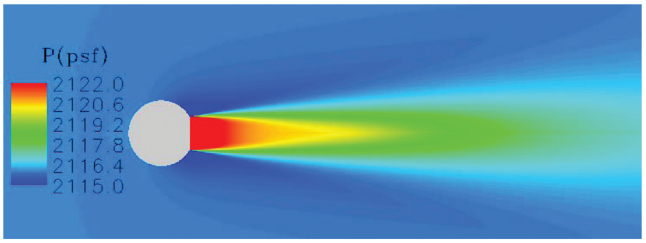

a)

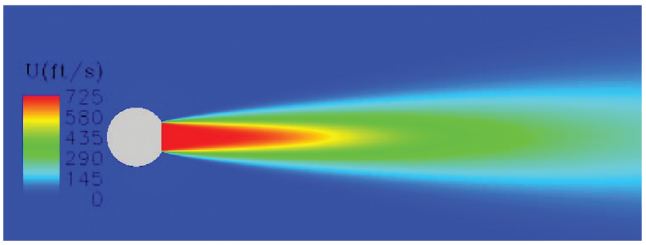

b)

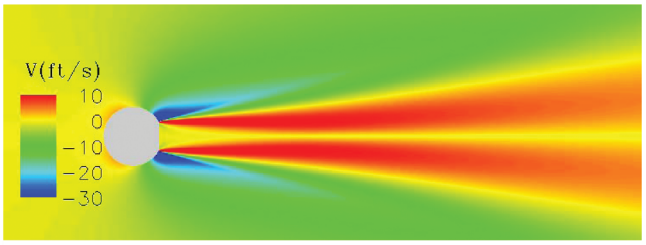

c)

Fig. 14 Jet exiting a spherical body: a) static pressures, b) axial velocities, and c) radial velocities.

for a jet from a round plenum, for which the spreading angle ranges between 5 and 7 deg depending on the test hardware [5]. The lateral velocity V, shown in Fig. 13c, shows entrainment into the jet (negative values of V) with the cool blue and green colors and spreading of the jet (positive values of V) with the warm red and yellow colors. The largest inflow velocities (< -30 fps) are located outside the jet boundary near the nozzle exit. The largest spreading velocities (>10 fps) are located inside the jet boundary but outside the potential core, and within the first 8–10 diameters from the jet exit. It is the combination of jet momentum conservation and the dissipation of jet kinetic energy by viscosity that causes the jet to entrain ambient fluid and increase its mass flow, as illustrated by the radial flows.

Jet from a Sphere

The computational results for the case with the sphere are presented in Fig. 14. This case was obtained for a jet exiting from a sphere for which the diameter is twice the jet diameter. For this case the initial total pressure of the jet was also prescribed to be 2857 psf, the same as the jet from the flat plate. The calculated static pressure distribution is presented in Fig. 14a. In this case, the static pressure at the nozzle exit was not specified to be 2116 psf; rather, it was determined as part of the solution. The static pressure at the jet exit rises above the ambient pressure, to 2132 psf. In the first diameter downstream of the exit, the static pressure reduces to 2120 psf and finally reaches ambient pressure 12 diameters downstream. The calculated axial velocity is presented in Fig. 14b and the radial velocity is presented in Fig. 14c. The potential core is only about 4.5 diameters long, about 0.5 diameters shorter than case of the flat plate. The radial entrainment velocities ($V < 0$ fps) are similar to those seen in Fig. 13c for the case of the flat plate. However, the radial spreading velocities ($V > 0$ fps) inside the jet cover a larger area and persist to a larger distance downstream (about 16 diameters) than in the flat plate case.

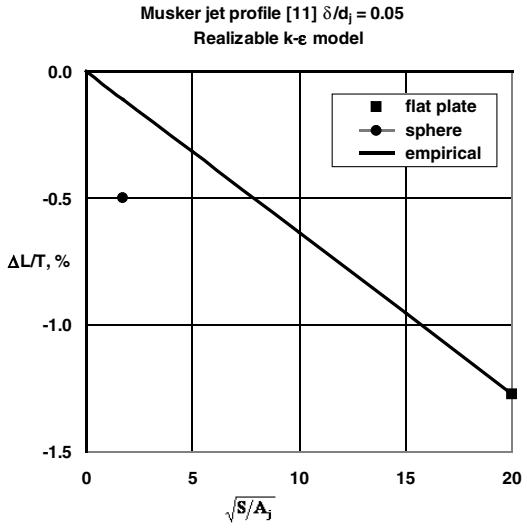

Fig. 15 Lift loss calculated by integration of the surface pressures on the sphere and flat plate.

Jet-Induced Lift Loss by Surface Pressure Integration

The computed results in Fig. 15 present the jet-induced lift loss determined in the present investigation by integrating the surface pressures. The spherical body has a projected area perpendicular to the jet direction that is 3 times the jet area. The flat plate has a projected area perpendicular to the jet direction that is 399 times the jet area. In Fig. 15, the data plotted at $\sqrt{S/A_j}$ of 1.73 are for the sphere and the data plotted at $\sqrt{S/A_j}$ of 19.98 are for the flat plate. The line represents the empirical variation of jet-induced lift loss due to reduced plate area S.

The potential core length of the jet can be adjusted to match experimental potential core lengths and jet decay slopes by changing the turbulence intensity. It is seen that the curve does not go to zero when $\sqrt{S/A_j}$ goes to zero, as expected from the experimental data. The induced lift loss for the plug flow was also computed and is compared with both the original and modified empirical correlation equation in Table 2.

Comparing these calculations to the modified empirical equation leads to several observations:

1) The jet solution for the constant total pressure profile underestimates the lift loss by about a factor of 2.

2) The jet solution for the Musker profile [11] from the flat plate gives a lift loss close to the empirical result.

3) The jet solution for the Musker profile [11] from the sphere gives a lift loss much larger than the value predicted by the empirical equation.

This last result for the lift loss computed for the sphere may explain why the $\Delta L/T$ curve in Fig. 11 is greater than zero when $\sqrt{S/A_j}$

Table 2 Comparison of computed lift loss with empirical equations

	$\Delta L/T$, %		
Case	Computational fluid dynamics	Original correlation equation	Modified correlation equation
Flat plate with constant P_T profile jet	−0.43	−2.0	−1.0
Flat plate with Musker profile jet [11]	−1.25	−2.0	−1.0
Sphere with Musker profile jet [11]	−0.50	−0.17	−0.085

goes to zero. It reveals that there is significant lift loss even though the flow around the spherical body does not separate.

Conservation of Momentum in the Numerical Solution

In the nozzle exit plane, the forces consist of the jet thrust and the jet-induced suction on the body:

$$T\text{-}D = \int (\rho U^2 - P_{\text{ref}} + P)\, \mathrm{d}A_j - \int (P_{\text{ref}} - P)\, \mathrm{d}(A - A_j)$$

As the static pressures return to the ambient pressure, P_{ref}, downstream of the nozzle exit, the net force must be the same in every downstream plane, because it is equal and opposite to the net force on the body due to the jet thrust and suckdown. Figure 16 shows the ratio of computed net force as a function of downstream distance to the initial net force at the jet exit, as a check on the accuracy of the numerical solution. This check is important because the results in the next section depend on calculating a small difference between two relatively large forces. The computed solution shows that the total momentum is conserved as the jet spreads and the static pressure relaxes downstream of the nozzle exit.

Loss of Jet Thrust by Integration of Velocity Profiles

Integration of the surface pressures on the flat plate yields a pressure drag of approximately 3 lbf. Because of the presence of the plate, the static pressure within the jet is higher than the static pressure at infinity. Therefore, integration of the jet velocity profile at the nozzle exit yields the jet momentum flux, which is not the same as the thrust of the jet, due to the increased static pressure. We will define the thrust of the jet at each streamwise location, T^*, as the thrust that would be obtained by an isentropic expansion (without additional mixing) of the local mass flux within the jet to the static pressure at infinity:

$$T^* = \int \rho U_i^2\, \mathrm{d}y_i$$

in which U_i prescribes the velocity profile of the jet after the isentropic expansion to the static pressure at infinity. At the nozzle exit, T^* will be equal to the thrust of the isolated jet, as if it had exhausted to ambient pressure in the absence of the flat plate. Far downstream of the nozzle exit, T^* will be equal to the thrust of the isolated jet minus the drag that the jet actually induces on the plate.

Because the expansion of the jet is assumed to occur without entrainment, the jet mass flux at infinity is equal to the local jet mass flux at the streamwise location being evaluated. The continuity equation for each expanding stream tube in the jet then yields

$$\int \rho U_i\, \mathrm{d}y_i = \int \rho U\, \mathrm{d}y$$

in which U_i prescribes the expanded velocity distribution and U prescribes the actual local velocity distribution. Therefore, the local thrust can be written

$$T^* = \int \rho U U_i\, \mathrm{d}y$$

Then, because U_i is defined by Bernoulli's equation,

$$P + 1/2\rho U^2 = P_\infty + 1/2\rho U_i^2$$

the thrust of the jet after expansion can be expressed in terms of the local jet velocity distribution at each streamwise location and the local static pressure:

$$T^* = \int \rho U[U^2 - 2(P - P_\infty)/\rho]^{1/2}\, \mathrm{d}y$$

In the flow outside of the jet

$$U^2 = 2(P - P_\infty)/\rho$$

so that this thrust integral differs from zero only within the jet. As a result, the jet thrust after expansion can be evaluated from the local velocity distribution and static pressure at each streamwise location. A similar equation is often used for evaluating airfoil drag from wake survey data near an airfoil, where the static pressure is different from the pressure at infinity due to the presence of the airfoil.

The computed streamwise variation of the jet thrust is shown in Fig. 17. The net force on the body is approximately $T\text{-}D = 25$ lbf. This is shown as a horizontal line, because it is a constant. The initial thrust of the jet at the nozzle exit is approximately 28 lbf. The 3 lb difference represents the flat-plate-induced pressure drag. It can be seen that the jet thrust approaches the net thrust asymptotically, as the effect of the sink drag accumulates. The surprising result is that the influence of the plate extends nearly 30 jet diameters downstream.

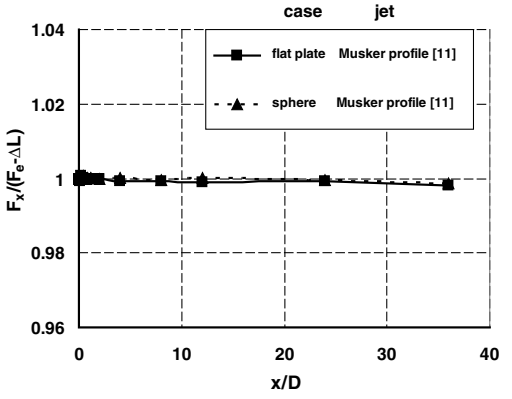

Fig. 16 Conservation of momentum in the solution for the jets from the flat plate and sphere.

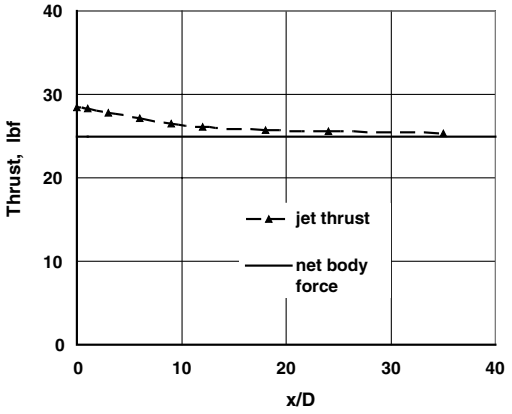

Fig. 17 Analysis of the flat plate case with Musker profile [11], $\delta/d = 0.05$ for a nozzle pressure ratio of 1.35.

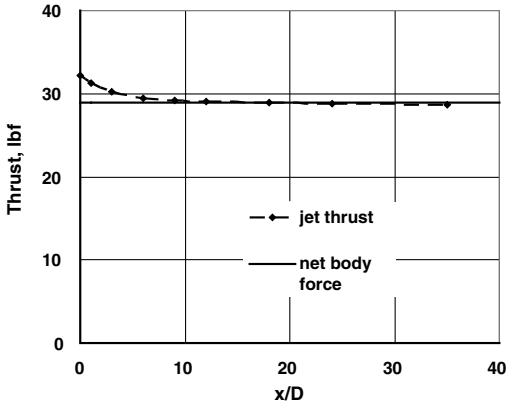

Fig. 18 Analysis of the sphere case with Musker profile [11], $\delta/d = 0.05$ for a nozzle pressure ratio of 1.35.

The analogous streamwise variation of the jet thrust for the case of the sphere is shown in Fig. 18. Even though the sphere is smaller than the plate, integration of the surface pressures yields almost the same pressure drag of approximately 3 lbf. This suggests that most of the suckdown is created by the very low pressures in the immediate vicinity of the nozzle exit. The initial jet thrust is close to 32 lbf. The net force on the body is a little less than $T\text{-}D = 29$ lbf in this case. This is shown as the horizontal line. The jet thrust approaches its asymptotic value at about the same rate as in the case of the flat plate, because the jets are similar and entrain ambient fluid at essentially the same rate. The influence of the sphere extends about 15 diameters downstream, half as far as the influence of the flat plate.

The computational results can be summarized as follows. The net force on either the sphere or the flat plate consists of the initial thrust of the jet and an induced pressure drag. Integration of the momentum flux and static pressure over control surfaces normal to the flow at any streamwise station has shown that the sum of the these quantities is constant and always equal to the net force on the bodies. However, the thrust of the jet decreases as the distance from the nozzle exit increases, until the net thrust far downstream is equal to the net force on the bodies. It should be noted that, as the static pressure in the jet drops to ambient pressure, the velocities in the jet are also dropping, so that the relaxation of the jet is different from the isentropic flow process described by Bernoulli's equation. The mechanism by which the induced pressure area force on the body acts to reduce the jet thrust is a pressure drag, similar to a sink drag, which acts against the jet along its length. This force is induced by the body and decreases as the distance from the body increases.

It is not necessary to accurately integrate the small pressure forces over the entire control surface to determine the net force on the body. It is sufficient to integrate the velocity distribution within the jet and calculate the isentropic thrust that would be obtained by expanding

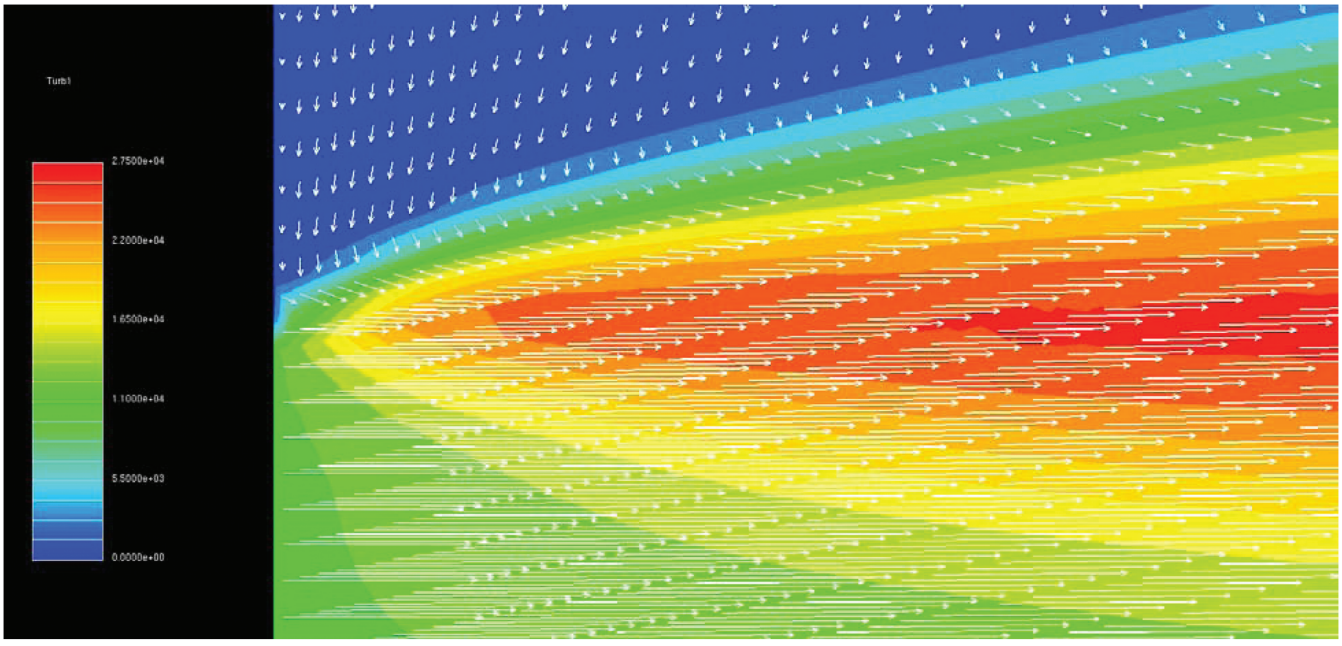

a)

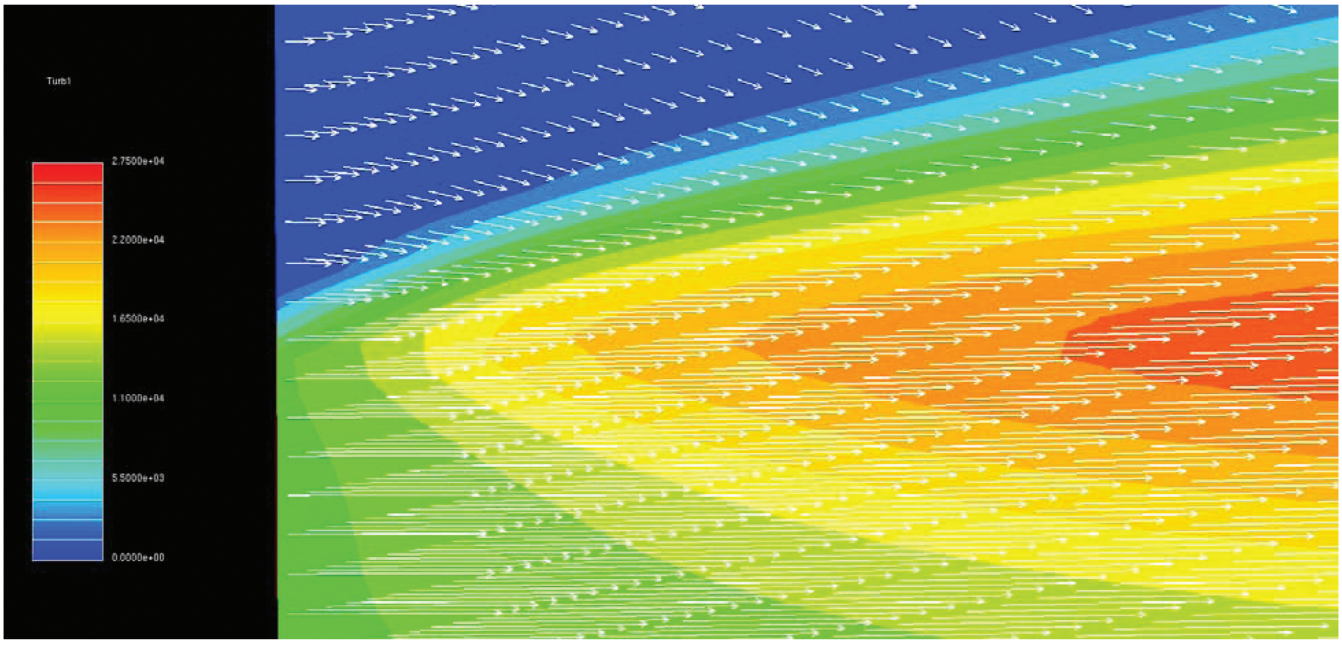

b)

Fig. 19 Turbulence kinetic energy (ft^2/s^2) in the initial shear layer of the jet: a) from a plate, and b) from a pipe.

the jet mass flow to the ambient pressure. The asymptotic value of the jet thrust is the net force on the body.

Loss of Jet Thrust to Turbulence Kinetic Energy

Because the reaction to the jet-induced suckdown on a body is a corresponding reduction in jet thrust, more of the kinetic energy of the mean jet flow must be dissipated in the jet from a finite body than would be dissipated in the jet from a thin-walled pipe, which has essentially no base area and therefore experiences no suckdown force. At high Reynolds numbers, the kinetic energy lost from the mean flow first goes into the kinetic energy of the turbulence, and then the turbulence ultimately dissipates it as heat by viscous action. Consequently, the production of turbulence in the jet issuing from a flat plate should be greater than it is in the jet issuing from a pipe.

Figure 19 compares the calculated turbulence kinetic energy produced in the shear layer of the jet from a flat plate (the case shown in Fig. 13) to the calculated turbulence kinetic energy produced in the shear layer of the jet from a very thin-walled pipe. The length of the region shown is approximately 15% of the nozzle radius. This region just downstream of the nozzle exit is where the interaction between the jet and the body is strongest and the loss of jet thrust is greatest, as seen in Figs. 17 and 18. Therefore, the difference in turbulence production should be greatest in this region.

The difference in the gradients of the colors shows that the kinetic energy of the turbulence does increase more rapidly and reach a higher peak value in the jet from the flat plate than it does in the jet from the thin-walled pipe. This confirms that more of the mean flow kinetic energy is lost to turbulence in the jet from the flat plate, which is consistent with the mechanism described in this paper. The additional kinetic energy lost from this jet is due to the fact that the mixing occurs in a high-pressure region; this increased loss of kinetic energy from the mean flow of the jet that exhausts from the flat plate results in a reduction of thrust compared to a jet that exhausts directly to atmospheric pressure.

Conclusions

Computational fluid dynamics has been used to provide an improved understanding of the physical mechanism of jet-induced thrust loss on hovering VSTOL aircraft. The jet solutions best matched the experimental data for the jet potential core length and the jet entrainment velocity flowfield with the use of a two-equation k–ε turbulence model, a nonuniform jet exit velocity profile with a finite boundary-layer thickness, and a 20% turbulence intensity. Grid and turbulence sensitivity studies showed that the solution depended on the grid size when the turbulence intensity was less than 10% of the mean jet velocity. However, when the turbulence intensity was increased to 20% of the jet velocity, there was virtually no effect of increasing the number of cells beyond 66,677 cells. This is probably because turbulent diffusion became significantly larger than the artificial numerical diffusion due to grid size.

If the static pressure in the nozzle exit plane is forced to be equal to the ambient pressure, the solution for the development of the jet is inaccurate. Within the first diameter of the exit, the static pressure in the jet rises to a value above ambient pressure and then slowly decays back to ambient pressure. This behavior produces an incorrect solution for turbulence production in the vicinity of the nozzle, where entrainment has the greatest influence on the predictions of the induced pressure drag. To obtain a correct prediction, the static pressure in the nozzle exit must be a floating boundary condition, which can rise to a value above ambient pressure at the nozzle exit as the flow adjusts to the increased static pressures induced in the jet by its own entrainment.

Integration of the momentum flux and pressure area term over control surfaces normal to the flow at any streamwise station confirmed that the sum of the these quantities is constant and always equal to the net force on the airframe. However, the thrust of the jet was observed to asymptotically decrease with distance from the airframe. For the case of the flat plate, the thrust changed over a distance of about 30 nozzle diameters from its initial value at the nozzle exit to a value equal to the net force on the airframe. For the sphere, the thrust reached its asymptotic net value after a distance of about 15 nozzle diameters.

The mechanism of the jet-induced thrust loss is an interaction between pressure forces on the airframe and the lift jets. This interaction induces a base pressure drag on the airframe and an equal but opposite pressure drag that acts against the jet along its length, reducing its thrust. This jet drag is due to the entrainment and mixing of ambient air by the lift jet in the high-pressure region created at the nozzle exit by the presence of the airframe. The loss of jet mean flow kinetic energy to turbulence increases in this high-pressure region, reducing the jet thrust. This jet drag is conceptually similar to the drag induced on a sink in an external stream.

Acknowledgments

Metacomp Technology, Inc. has provided very essential support to this investigation; the assistance of Paul Batten is especially appreciated. Our colleague, Ali Hadid, assisted in interpreting the computational results; his questions stimulated a deeper examination of the basic concepts in this paper.

References

[1] Albertson, M. L., Dal, Y. B., Jensen, R. A., and Rouse, H., "Diffusion of Submerged Jets," *Transactions of the American Society of Civil Engineers*, Vol. 115, 1950, pp. 639–697.

[2] Wyatt, L. A., "Static Tests of Ground Effect on Planforms Fitted with a Centrally-Located Round Lifting Jet," Aeronautical Research Council, CP 749, U.K. Ministry of Aviation, June 1962.

[3] Shumpert, P. K., and Tibbetts, J. G., "Model Tests of Jet-Induced Lift Effects on a VTOL Aircraft in Hover," NASA CR-1297, March 1969.

[4] Kuhlman, J. M., Ousterhout, D. S., and Warcup, R. W., "Experimental Investigation of Effect of Jet Decay Rate on Jet-Induced Pressures on a Flat Plate," NASA CR-2979, April 1978.

[5] Gentry, G. L., and Margason, R. J., "Jet-Induced Lift Losses on VTOL Configurations Hovering In and Out of Ground Effect," NASA TN D-3166, Feb. 1966.

[6] Kuhn, R. E., Bellavia, D. C., Wardwell, D. A., and Corsiglia, V. R., "On the Anomalies in Single-Jet Hover Suckdown Data," NASA TM 102261, Aug. 1991.

[7] Ousterhout, D. S., "An Experimental Investigation of a Cold Jet Emitting from a Body of Revolution into a Subsonic Free Stream," Old Dominion Univ. NASA CR 2089, Aug. 1972.

[8] Kuhn, R. E., Margason, R. J., and Curtis, P., *Jet-Induced Effects: The Aerodynamics of Jet- and Fan-Powered V/STOL Aircraft in Hover and Transition*, Vol. 217, Progress in Astronautics and Aeronautics, AIAA, Reston, VA, 2006.

[9] Chakavarthy, S., "Realizing High Fidelity Computational Simulations of Fluid Dynamic Phenomena," *Computational Fluid Dynamics Journal*, Vol. 16, No. 4, April 2008, pp. 356–362.

[10] Husain, Z. D., and Hussain, A. K. M. F., "Axisymmetric Mixing Layer: Influence of the Initial and Boundary Conditions," *AIAA Journal*, Vol. 17, No. 1, Jan. 1979, pp. 48–55. doi:10.2514/3.61061

[11] Musker, A. J., "Explicit Expression for the Smooth Wall Velocity Distribution in a Turbulent Boundary Layer," *AIAA Journal*, Vol. 17, June 1979, pp. 655–657. doi:10.2514/3.61193

[12] Palaniswamy, S., Goldberg, U., Peroomian, O., and Chakavarthy, S., "Predictions of Axial and Transverse Injection into Supersonic Flow," *Flow, Turbulence and Combustion*, Vol. 66, 2001, pp. 37–55. doi:10.1023/A:1011479002452

[13] Tennekes, H., and Lumley, J. L., *A First Course in Turbulence*, MIT Press, Cambridge, MA, 1972, p. 110.

[14] Babu, P. C., and Mahesh, K., "Upstream Entrainment in Numerical Simulations of Spatially Evolving Round Jets," *Physics of Fluids*, Vol. 16, No. 10, Oct. 2004, pp. 3699–3705. doi:10.1063/1.1780548

E. Livne
Associate Editor